RESEARCH ARTICLE | AUGUST 02 2024

Prediction and sensitivity analysis of the pressure wave peak value induced by the high-speed train in the long tunnel under a high geothermal environment

Special Collection: Flow and Civil Structures

Junyan Wang (王军彦) ; Tiantian Wang (王田天) ; Yiping Wang (汪怡平) ; Chihyung Wen (溫志湧) ; Lei Zhang (张雷) ; Zhikun Sun (孙志昆)

Physics of Fluids 36, 086106 (2024)
https://doi.org/10.1063/5.0216631

Physics of Fluids ARTICLE pubs.aip.org/aip/pof

Prediction and sensitivity analysis of the pressure wave peak value induced by the high-speed train in the long tunnel under a high geothermal environment

Cite as: Phys. Fluids **36**, 086106 (2024); doi: 10.1063/5.0216631
Submitted: 30 April 2024 · Accepted: 18 July 2024 ·
Published Online: 2 August 2024

View Online Export Citation CrossMark

Junyan Wang (王军彦),[1,a)] Tiantian Wang (王田天),[2,3,a)] Yiping Wang (汪怡平),[1,a)] Chihyung Wen (溫志湧),[4] Lei Zhang (张雷),[2] and Zhikun Sun (孙志昆)[2]

AFFILIATIONS

[1]Hubei Key Laboratory of Advanced Technology for Automotive Components, Wuhan University of Technology, Wuhan 430070, China
[2]Key Laboratory of Traffic Safety on Track, Ministry of Education, School of Traffic & Transportation Engineering, Central South University, Changsha 410075, China
[3]College of Mechanical and Vehicle Engineering, Hunan University, Changsha 410082, Hunan, China
[4]The Hong Kong Polytechnic University, Department of Aeronautical and Aviation Engineering, Hung Hom, Kowloon, Hong Kong, China

Note: This paper is part of the special topic, Flow and Civil Structures.
[a)]**Authors to whom correspondence should be addressed:** jywangwl@whut.edu.cn; wangtiantian@csu.edu.cn; and wangyiping@whut.edu.cn

ABSTRACT

Pressure changes outside a train can be transmitted into a carriage when the train is running in the tunnel, seriously affecting passenger comfort. In this paper, the polynomial response surface (PRS) is used to predict the value of the compression wave and obtain the predictive model equations. For the traveling pressure waves, many influencing factors contribute differently to the final pressure wave form and magnitude. In geothermal tunnels, the speed of a high-speed train (V), air temperature of the inner tunnel (T), and atmospheric pressure (P) are the three main influencing parameters. Using a PRS prediction model, the sensitivity of each influencing parameter is analyzed by the Sobol sensitivity method. The result shows that V has the greatest effect on the pressure peak value, and T has the least effect. The initial compressional waves and expansion waves are most and least sensitive to T, respectively. The coupling effect among parameters P, T, and V is relatively small. Using the sensitivity results of the parameters, targeted and reasonable parameter adjustment can effectively relieve the pressure inside and outside the train and improve passenger comfort in geothermal tunnels. These results provide important technical support for the mitigation of pressure waves.

I. INTRODUCTION

In China, newly built railways with speeds of 250–350 km/h are called high-speed railways, and some 200 km/h railways have also been incorporated into the Chinese high-speed rail network. There are many factors that affect pressure waves, such as the train speed, atmospheric pressure, train length, and tunnel length. For geothermal tunnels, temperature is also a significant factor to pressure waves. The Sichuan–Tibet railway line is an extremely important engineering project in Chinese traffic research. In Tibetan areas, long geothermal tunnels are very common.[1] The maximum temperature of the rock can exceed 89.6 °C in a high-temperature geothermal tunnel, causing the tunnel air temperature of 56 °C. Most geothermal tunnels are long, so the traveling pressure waves in the tunnels can become relatively complex. Therefore, the various influencing factors to a pressure wave need to be studied, also it is necessary to explore whether there is a coupling relationship between them.

Recent studies on the aerodynamics of railway tunnels have mainly concentrated on normal temperature conditions. For characteristics of pressure waves, most studies have focused on the evolution law and formation mechanism of pressure waves by experiments and

simulations. Experimental research is primarily carried out with a scaled model. Using 1/8,[2] 1/20,[3,4] and 1/25[5,6] scaled moving models, researchers have carried out experiments on trains passing through tunnels or confined spaces. The aerodynamic performance for different trains and tunnels and the law of transient pressure generated by high-speed trains were obtained. For numerical simulations, the evolution of flow fields as a train passes through a tunnel at normal temperature was mainly investigated, with various trains and tunnel parameters. Iyer *et al.*[7] studied the waveform distortion and nonlinear distortion of the waveform during the formation of compressed waves and obtained the waveform change law caused by the nonlinear distortion. Li *et al.*[8] carried out a study on the aerodynamic mechanism of the micro-pressure wave buffer structure at the mouth of a 400-km railway tunnel. Liu *et al.*[9] studied the effect of circumferential cracks in the lining of high-speed railway tunnels on the initial compression wave. Due to the limited airspace within a tunnel, considerable transient pressure waves are generated when a high-speed train passed through it, leading to passenger discomfort.[10] The pressure gradient of tunnel compression waves is noted as a key issue. Wang *et al.*[11] studied the propagation of weak shock waves at the tunnel exit and the influence of micro-pressure waves on tunnel buildings. Miyachi *et al.*[12] studied the nondimensional maximum pressure gradient with experiments and theoretical derivations. The above-mentioned studies on pressure waves in tunnels have focused on normal temperature conditions and have not considered the influence of high-temperature geothermal conditions. This paper will construct experimental and numerical simulation methods for high geothermal tunnel environments, establish a pressure wave prediction model, and conduct sensitivity research on influencing factors, and to explore the influence weight of each influencing factor on the pressure wave. Additionally, there is a lack of research methodology and simulation models for high-temperature geothermal tunnel environments. Therefore, it is necessary to further improve the existing research tools.

Researchers have also conducted related research for high altitude and cold-temperature conditions in railway tunnels. Luo[13] studied the effects of atmospheric pressure and temperature at high altitude on the aerodynamic characteristics of high-speed railway tunnels. However, the gradient of temperature in the tunnel and the random distribution of geothermal heat are not taken into account. Because of high altitudes and geothermal tunnel being prone to freezing damage, a lot of research methods have developed in recent years.[14] The research on the temperature field in high-altitude tunnels mainly focuses on the seasonal changes of temperature fields and related tunnel facilities insulation. Dai *et al.*[15] studied the influence of temperature change brought by altitude on tunnel pressure wave. Using field measurements in cold regions, researchers have studied the thermal insulation technology and temperature field theory of railway tunnels.[16] Many scholars have also studied the thermal convection inside tunnels in cold regions. Zeng *et al.*[17] and Zhou *et al.*[18] carried out related studies on heat convection–conduction for rock and wind currents. The above-described studies on tunnels in the alpine regions of the plateau mainly focused on the tunnel insulation layer, the convective heat transfer inside the tunnel, and the change in the tunnel temperature field. However, research on the transient pressure when the train pass through the geothermal tunnel is rare, so it is necessary to explore and study the transient pressure behavior in this environment.

In summary, the existing research has mainly focused on pressure wave changes in the tunnel environment at normal temperature. Since the simulation of the initial temperature field is the main difficulty, the simulation of high geothermal tunnels is difficult to achieve, so there are few studies on this aspect at present. Few studies have investigated a predictive model of the pressure wave value, and a sensitivity analysis of the influencing parameters on the pressure results in high geothermal tunnels. In addition, the influence weight of the parameters on the pressure results is significant to mitigate pressure. The targeted and reasonable adjustment of parameters can effectively relieve the pressure inside a train and improve passenger comfort in geothermal tunnels, so it is necessary to carry out relevant research.

II. NUMERICAL SIMULATION

A. The setting of simulation to the heating zone

For a numerical simulation, a reasonable setting plays a significant role to the numerical results. Due to the particularity of the current simulation of the geothermal tunnel with a heating zone, the settings of the heating zone need to be particularly addressed. To obtain a precise temperature field, the simulation proceeds with the following steps:

(1) The train runs a distance outside the tunnel at a lower speed. (2) The train remains stationary, and the flow field is stabilized by calculation. (3) The train speed is maintained at 0 and the simulation of the initial temperature field is started by heating the tunnel wall surface. (4) The train then is running through the tunnel at the test speed. The specific process is shown in the Fig. 1.

B. Simulation method and boundary conditions

In this study, the characteristic of a flow field is three-dimensional, compressible, unsteady and turbulent flow, the train speed is 350 km/h, and the compressibility of the air cannot be ignored.[19] Nowadays, the Re-normalization group (RNG) $k-\varepsilon$ turbulence model is used for resolving the turbulence. Reynolds Averaged Navier–Stokes equations

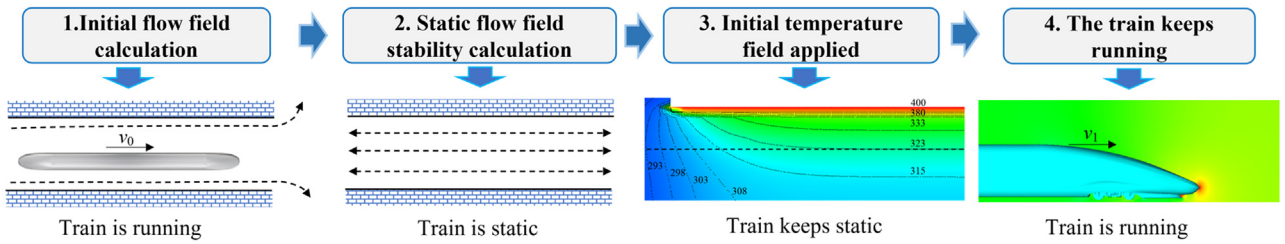

FIG. 1. Numerical simulation process of a high geothermal tunnel.

are used to solve computational fluid dynamics (CFDs).[20–24] Figure 2 is the simulation domain for the case of a train passing through a tunnel. As Fig. 2(a) shows, the simulation domain contains static (A and B) and sliding domains (the dotted line part C). The static domain mainly contains two open air zones, while the sliding domain is mainly the movement area composed of the train and the air domain around the train. Due to the presence of geothermal heating in this research, the tunnel area includes two parts, the heating and normal temperature zones. For the heating area, high geothermal conditions can be simulated by heating the tunnel wall. The static and sliding domains are connected by the interfaces. These dimensions can ensure that when the train moves in the open domain, the normal flow field at the domain boundary (i.e., the far field from the train) will not be affected, reflecting the real situation. As shown in Fig. 2(b), the boundary conditions are defined for the numerical simulation. The settings of computational boundary are shown in Fig. 2.

C. Computational grid

1. Meshing strategy

Figure 3 shows the computational meshes. Because the train contains complex components such as bogies and the train body surface, their nearby computational domains are discretized using a tetrahedron grid. The shapes of other areas are relatively regular, so that the grids are of a hexahedron grid in these parts. In order to make the simulation accuracy higher, the grids surrounding the train and nearby areas need further refinement. The minimum surface grid sizes

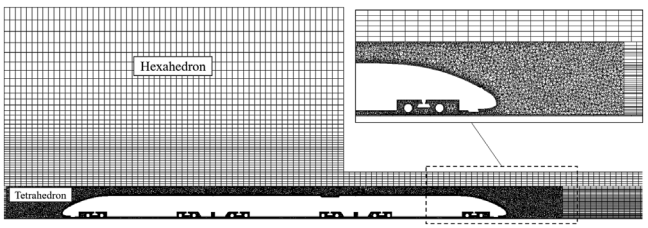

FIG. 3. Computational grids.

surrounding the bogies and train body are 6 and 10 cm, respectively, and that near the grid of the tunnel surface is 15 cm.

2. Grid and time step independence

To compare the influence of different grid scales on pressure results, the pressure changes at measuring points in the tunnel were analyzed. Figure 4(a) presents the pressure variation results. It is evident that the difference between the medium and fine grids is minimal, with the initial compression wave peak varying only by 0.39% and 0.84%, respectively. However, the coarse grid results significantly deviate from the other two grids, showing differences of 2.15% and 3.62% in initial compression wave peak values compared to the medium grid. To balance high mesh accuracy with computational efficiency, the medium mesh was selected for subsequent calculations. Additionally, the time step independence was verified by studying the effects of

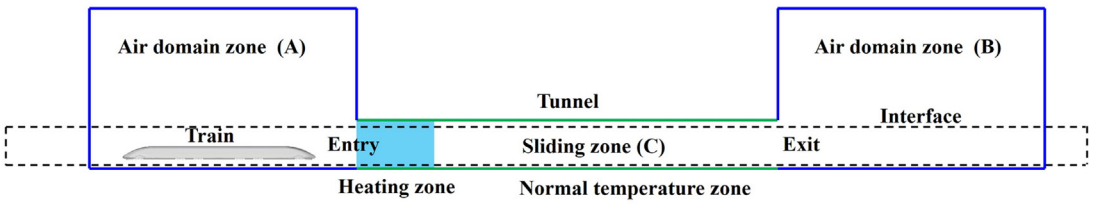

(a) Static part and sliding part

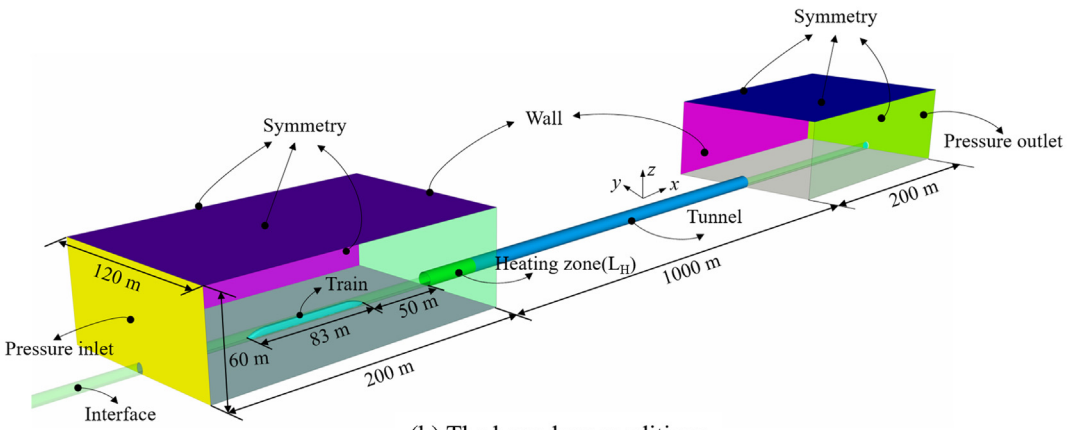

(b) The boundary conditions

FIG. 2. Simulation domain and boundary conditions.

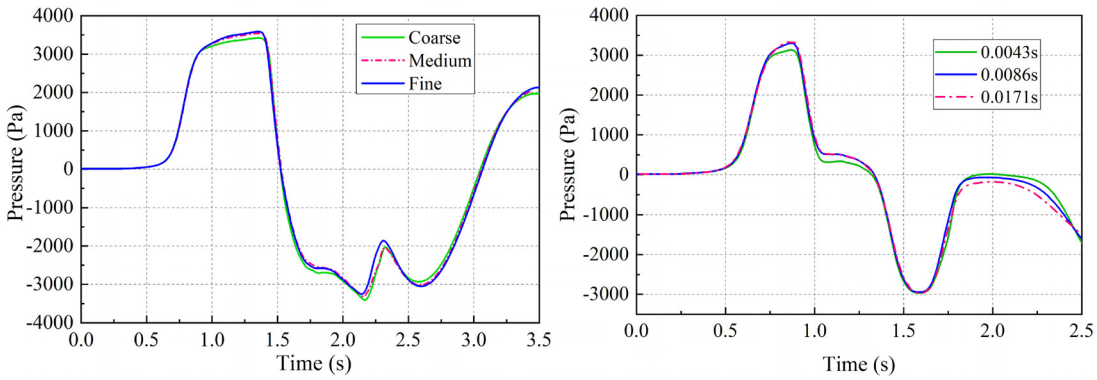

FIG. 4. The results of grid and time step independence.

different time steps (0.0043, 0.0086, and 0.0171 s) on the results, as shown in Fig. 4(b). It can be observed that results with time steps of 0.0086 and 0.0171 s are similar, closely resembling the experimental curves and effectively capturing pressure fluctuations. Considering the grid size in the tunnel length direction of 1 m and to align with the movement distance of each train step, a time step of 0.0086 s was chosen for further simulations.

III. EXPERIMENT AND COMPARISON

A. Moving model test

To study the influence of high geothermal conditions in tunnels on the propagating pressure waves, local heating tests were carried out in the model test platform. Figure 5 shows the models in the local heating moving model test, and the model is a 1/20 scaled down one in the experiment.[25] The tunnel real-scale cross section area is 70 m^2. The heating sheet is tightly connected to the inner wall of the tunnel and has a total length of 2 m from the tunnel entrance. The temperature sensor model is wzp-pt100 probe temperature sensor. The sensor response time is 0.5 s, and the measurement accuracy is $\pm(0.15 + 0.002|T|)°C$, where T is the measured temperature in degrees Celsius (°C). The pressure measurement sensor is the Honeywell DC030NDC4 pressure sensor. In this group of experiments, the sampling frequency of the sensor is 1 kHz, and the measurement accuracy is 0.01 Pa.

To conduct the local heating experiment, the moving model experiment is carried out when the temperature of the relevant measurement point reaches 323 K (50 °C). When using high-speed trains to conduct moving model experiments, the results of each test are then checked for accuracy. The accuracy criterion is that the difference between the experimental speed and the target speed of the train should not exceed 2%, the test results that do not meet this criterion will be excluded.

B. The comparison results of the measuring points

Figure 6 is a schematic diagram of the distribution of measurement points for high-speed train and tunnel. In this study, the pressure curves of two measurement points are shown in paper, and the measuring point is located in the normal temperature area in the middle of the tunnel. The measuring point H1 on the surface of the train is the first train measuring point with large flow separation, and the H2 measuring point is 3.22 m away from the nose tip of the first train.

Figure 7 shows the comparison results between the numerical simulation and the experiment. The pressure-time curves show that the experimental data of the moving model is in good agreement with

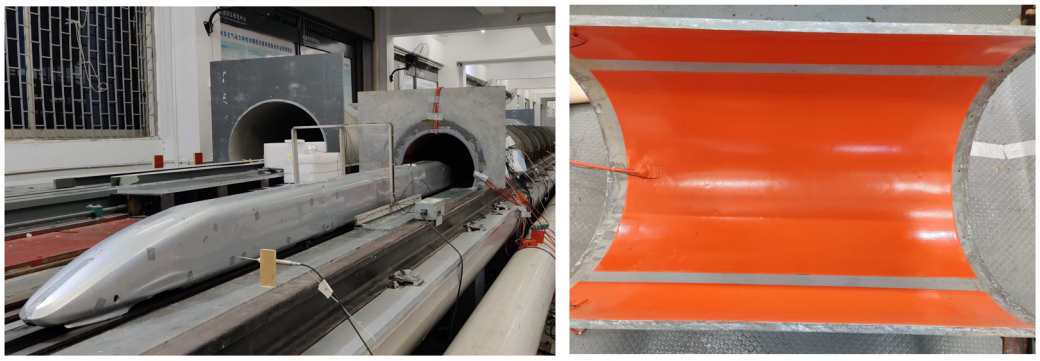

(a) The train model (b) The tunnel model with the heating surface

FIG. 5. Models of the moving train test.

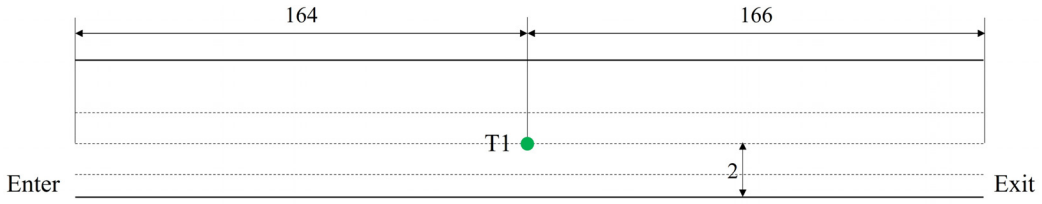

(a) The measuring point T1 in tunnel surface (unit: m)

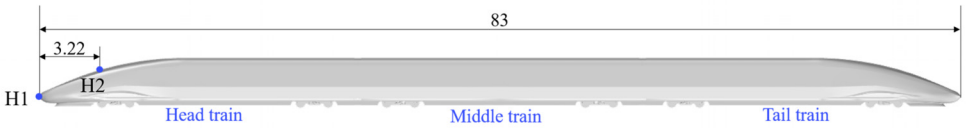

(a) The measuring point of train surface (unit: m)

FIG. 6. The measurement points of the tunnel and train (unit: m).

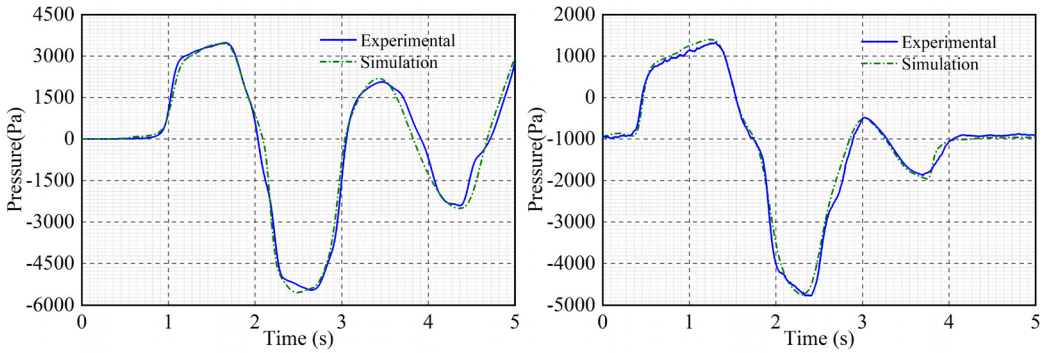

(a) T1 point (b) H2 point

FIG. 7. The comparison of experimental and numerical pressure wave results.

the numerical simulation data. In the numerical simulation, the drag and track friction are not considered, and the train running speed is unchanged, so the pressure peak value obtained by the experiment is slightly lower than that obtained by the numerical simulation. From the following experimental and numerical simulation results, it can be seen that the numerical difference of pressure is very small, and the difference is less than 2%. Therefore, the accuracy of the pressure results obtained by the numerical simulation method established in this study meets the research requirements.

Figure 8 is the initial geothermal field in the simulation computation. Points 1–4 in Fig. 8 are four measuring points of temperature measured before the moving model experiment. The positions of the four temperature measurement points in the numerical simulation correspond to those in the experiment. In addition, the ambient temperature of the simulation is also initially set according to the measured data during the experiment, so as to ensure that the boundary conditions of the experiment and the simulation are basically the same. As can be seen from Fig. 8, the heat is transferred from the tunnel wall to the air in the tunnel, and the temperature gradient is uniform, and the temperature value is basically consistent with the experimental data. As can be seen from Table I, the difference between the temperature data of the four measurement points and the experimental time is very small, all of which are less than 0.54%, indicating that the initial temperature field simulation has high accuracy. Therefore, the simulation algorithm is verified in the paper. In this paper, all the temperature values are the data of 0.2 m above the ground.

IV. RESULTS AND DISCUSSION

A. The tunnel length

According to the principles of pressure wave propagation and superposition, as shown in Fig. 9. This figure is a schematic diagram of the intersection of the expansion wave in the tunnel and the train body at a certain point in the tunnel. Through the figure, the meaning of the points shown can be intuitively understood, and the components of the expansion wave peak value can be observed in the figure, the maximum peak value of the initial expansion wave appears in the tunnel when the train and expansion wave (EW1) which is reflected by the compression wave pass first meets. However, this meeting point will

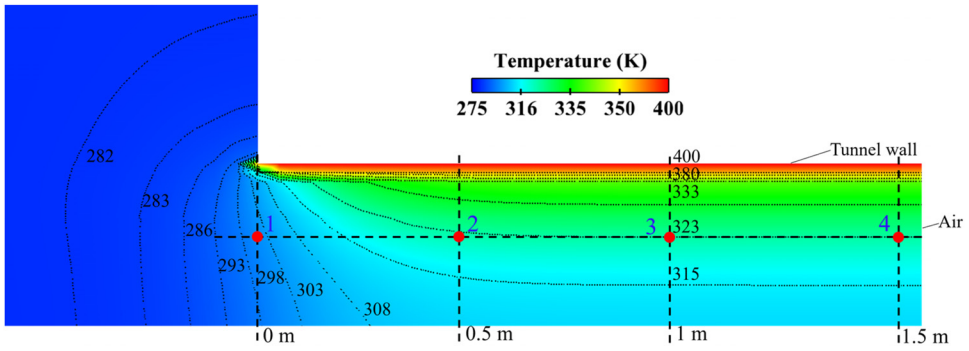

FIG. 8. Initial geothermal field.

TABLE I. Temperature results at different positions.

	0 m (K)	0.5 m (K)	1 m (K)	1.5 m (K)
Experimental value	298.3	322.6	322.9	324.8
Numerical value	297.5	322.0	323.0	323.0
Relative difference	0.28%	0.17%	0.03%	0.54%

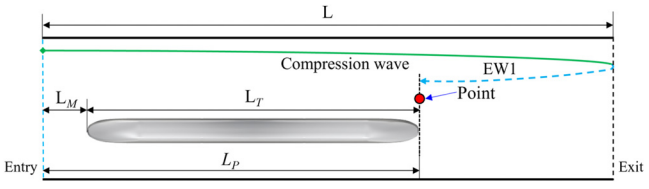

FIG. 9. Pressure wave propagation inside the tunnel.

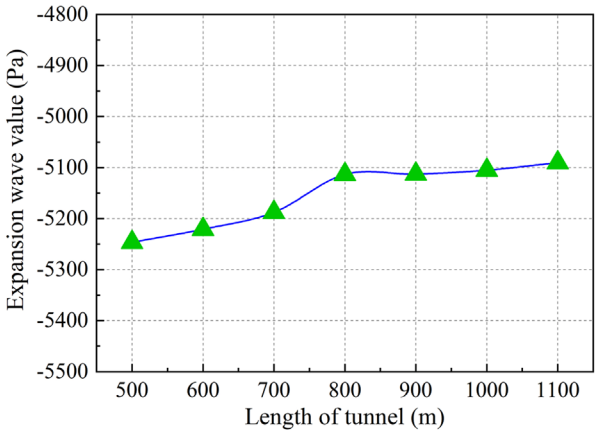

FIG. 10. The variation of the peak value of the expansion pressure with the length of tunnel at 350 km/h.

change with the tunnel length; therefore, the selection of tunnel length needs to be addressed. In this paper, the length of tunnel for the two extreme speed conditions of 200 and 350 km/h are studied.

1. Determining the tunnel length for train speed at 350 km/h

Figure 10 shows the variation of the peak value of the initial expansion pressure wave with the length of tunnel. As seen in Fig. 10, when the length of tunnel is more than 800 m, the peak value of the initial expansion pressure remains relatively constant.

2. Determining the tunnel length for train speed at 200 km/h

Figure 11 shows the trend of the peak value of the expansion wave with the tunnel length. When the tunnel length ranges from 500 to 900 m, the expansion wave peak value increases significantly, while when the tunnel length increases over 800 m, the increase trend gradually saturates. Notably, when the length ranges from 1000 to 1100 m, the pressure wave magnitude approaches basically a constant value.

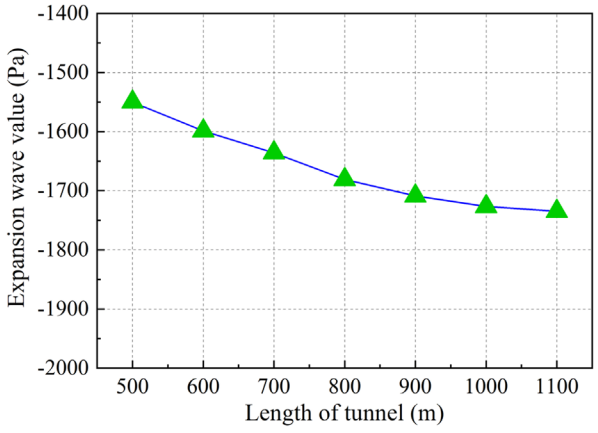

FIG. 11. The variation of the expansion pressure peak value with the tunnel length at a speed of 200 km/h.

From the above analysis, it can be seen that for train velocities at 200 and 350 km/h, the peak value of the expansion wave varies relatively insignificantly with the tunnel length when the tunnel length is over 800 m; In particular, when the tunnel length exceeds 1000 m, the pressure value variation is further reduced. Therefore, the tunnel length of 1000 m is selected for this study.

3. Initial expansion wave peak change trend analysis

From the above analysis results, it can be seen that the variation law of the peak value of the initial expansion wave is different under the two velocity conditions. When the speed is 350 km/h, the peak value of the initial expansion wave decreases with the increase in tunnel length, and when the velocity is 200 km/h, the trend of the initial expansion wave is that the tunnel length increases. This phenomenon will be analyzed next.

The position of the measurement point at the time of the initial expansion wave is shown in Fig. 9. According to the propagation law of the pressure wave, it can be obtained as

$$\frac{2L - L_P}{c} = \frac{L_M + L_T}{v_{tr}}, \tag{1}$$

$$L_P = \frac{2L \times v_{tr}}{c + v_{tr}}, \tag{2}$$

where v_{tr} is the velocity of train and c is the velocity of sound.

According to Eqs. (1) and (2), the position of the measurement point can be calculated under two different speed conditions, as shown in Table II.

TABLE II. The measurement points position of 350 and 200 km/h.

Tunnel length	500 m	600 m	700 m	800 m	900 m	1000 m	1100 m
Speed 200 km/h (m)	140	169	197	225	253	281	309
Speed 350 km/h (m)	222	267	311	356	400	445	489

As can be seen from the data in the table, at the train speed of 200 km/h, the superposition points are located closer to the front of the tunnel. From the pressure wave curves, it can be seen that when the train speed is 350 km/h, the expansion wave appears later. At this time, before the initial expansion wave is formed, the expansion wave generated by the rear of the train when it enters the tunnel has completely passed through the measurement point. As shown in the dotted box in Fig. 12, the measurement point will not be affected by the expansion wave, and the pressure wave will remain unchanged or rise briefly due to the friction between the train and the air. This upward trend will reduce the absolute value of the peak of the initial expansion wave. For the case of 200 km/h, as shown in Fig. 13, the pressure wave will continue to show a downward trend under the influence of the expansion wave generated when the tail train enters the tunnel due to the relatively high superposition point. So, in this case, the absolute value of the initial expansion wave peak will become larger.

B. Predictive models and error analysis

1. Mathematical principles

In reality, different engineering products presents different levels of complexity. To obtain efficient and accurate optimization engineering designs, an efficient approach is to adopt a surrogate model.[26]

The polynomial response surface (PRS) model is widely used in prediction and optimization studies. The approximate function of the PRS model is shown in the following equation:

$$b_0 + \sum_{i=1}^{n} b_i x_i + \sum_{i=1}^{n} \sum_{j=1}^{n} b_{ij} x_i x_j + \sum_{i=1}^{n} \sum_{j=1}^{n} \sum_{k=1}^{n} b_{ijk} x_i x_j x_k. \tag{3}$$

The design of experiment sampling points and basic functions introduce numerical errors. Metrics such as the mean relative error (*MRE*), maximum error (*ME*), root mean square error (*RMSE*), and coefficient of determination (R^2) can be used to evaluate the accuracy of these predictive models. These metrics are defined as follows:

$$MRE = 100\% \times \frac{\sum |(\tilde{y}_i - y_i)/y_i|}{n}, \tag{4}$$

$$ME = 100\% \times Max|(\tilde{y}_i - y_i)/y_i|, \tag{5}$$

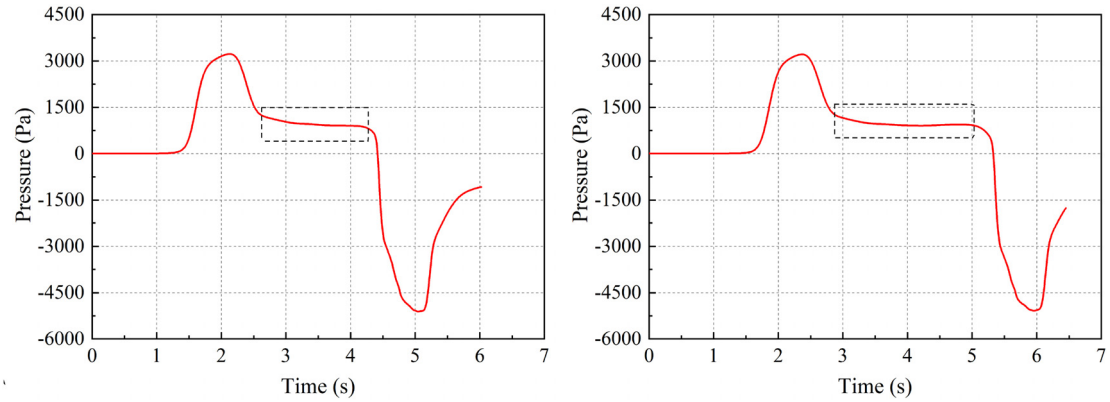

FIG. 12. Variation of pressure at different lengths of tunnels at a speed of 350 km/h.

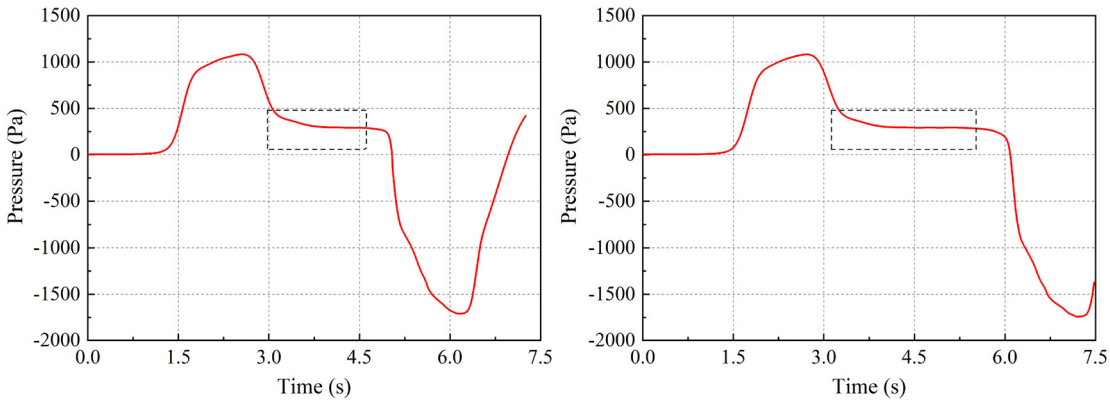

FIG. 13. The variation of pressure at different lengths of the tunnel at 200 km/h.

$$RMSE = \sqrt{\frac{\sum (\tilde{y}_i - y_i)^2}{n}}, \tag{6}$$

$$R^2 = 1 - \frac{\sum (\tilde{y}_i - y_i)^2}{\sum (y_i - \bar{y})^2}, \tag{7}$$

where n is the sample points number, y_i and $\tilde{y}_i$ are the simulation results and the predictive model value at every point i, and $\bar{y}$ is the average response of the numerical simulation. When the R^2 is closer to 1, the predictive model has higher accuracy. Meanwhile, smaller *MRE*, *ME* and *RMSE* values indicate a better predictive model.

2. The predictive model of the PRS

This research mainly focuses on the strengths of the compression wave (*C. P*), expansion wave (*E. P*) and the corresponding peak-to-peak (*P. P*). For pressure waves, train shape, tunnel structure and materials do have an impact on the size and propagation of pressure waves. However, the cross-sectional areas of trains and tunnels in actual operation are mostly fixed and do not change much, therefore, they were not included in the main research objects. The material of trains and tunnels has little effect on pressure waves and is therefore not considered. Therefore, the predictive models are also concentrated on the three targets. For a high geothermal tunnel, the main factors influencing the pressure wave value are atmospheric pressure (P), train speed (V), air temperature in the tunnel (T) and length of the tunnel. According to the altitude of the Sichuan–Tibet Railway, the minimum atmospheric pressure P will be close to 0.5 atm, so the research range of atmospheric pressure is 0.5–1 atm. The train speed in the plateau area can reach 200 km/h, and the running speed in the plain area can be 350 km/h. Therefore, the train speed V is selected from 200 to 350 km/h. The air temperature of the high geothermal tunnel can reach 56 °C, and the normal temperature in most tunnels is generally 20 °C. To make the applicable range of the temperature relatively large, the temperature T is selected between 10 and 60 °C. Because the tunnel length has been determined as a fixed length earlier, this predictive model study mainly investigates the atmospheric pressure P, train speed V and the air temperature of the inner tunnel T. The mathematical model of the predictive issue on the PRS is

$$\left\{ \begin{array}{c} [C.P(P,T,V), E.P(P,T,V), P.P(P,T,V)] \\ 0.5\,\text{atm} \le P \le 1\,\text{atm} \\ 10^{\circ}\text{C} \le T \le 60^{\circ}\text{C} \\ 55.56\,\text{m/s} \le V \le 97.22\,\text{m/s} \end{array} \right\}. \tag{8}$$

3. Design of the experiment

Design of experiment (DOE) methods are used in model prediction sampling, especially those with interfactor interactions.[27] Common DOE methods include Latin hypercube designs (LHD), orthogonal arrays, and optimal Latin hypercube designs (Opt LHD). Opt LHD allows all sampling points to be distributed uniformly and with very good space filling and balance, so this method is widely used. Figure 14 illustrates the distribution of sample points for Opt LHD, and Table III lists the values obtained by the simulations.

4. Predictive results and error analysis

Based on the results of the numerical simulation for the DOE sampling points, the PRS predictive models of the *C. P* (compression

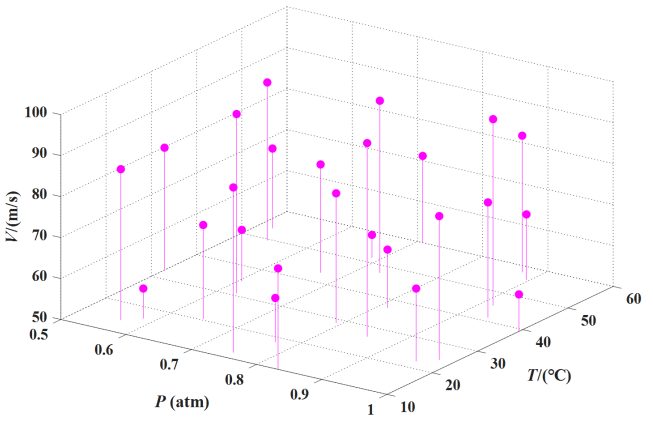

FIG. 14. The distribution of sample points for Opt LHD.

TABLE III. The sample points of DOE and simulation values.

No.	Atm.	Temperature (°C)	Speed (m/s)	C. Peak	E. Peak	P-P value
1	0.75	12.08	90.28	2050	−3379	5342
2	0.521	53.75	69.45	771	−1349	2109
3	1.0	39.17	59.03	1086	−1877	2951
4	0.854	26.67	97.22	2644	−4388	6979
5	0.792	28.75	81.6	1693	−2885	4553
6	0.938	41.25	78.13	1773	−3097	4847
7	0.625	30.83	93.75	1775	−2983	4725
8	0.542	49.58	88.54	1300	−2267	3548
9	0.563	14.17	86.8	1411	−2342	3733
10	0.667	43.33	76.39	1200	−2099	3284
11	0.771	18.33	60.77	937	−1574	2500
12	0.958	22.5	67.71	1427	−2418	3827
13	0.813	37.08	64.24	1052	−1813	2851
14	0.708	60.0	71.18	1057	−1896	2938
15	0.729	47.5	92.01	1906	−3292	5167
16	0.5	32.92	79.86	1014	−1741	2740
17	0.646	20.42	72.92	1123	−1901	3008
18	0.875	57.92	83.33	1804	−3221	5001
19	0.979	24.58	85.07	2295	−3885	6149
20	0.583	16.25	57.3	634	−1060	1687
21	0.688	51.67	55.56	642	−1123	1758
22	0.917	45.42	95.48	2609	−4469	7028
23	0.604	35.0	62.5	745	−1279	2014
24	0.833	10.0	74.65	1628	−2652	4257
25	0.896	55.83	65.98	1160	−2036	3181

wave), *E. P* (expansion wave), and *P. P* (peak-peak value) for the factors *P*, *T*, and *V* are obtained. Equations (9)–(11) are the predictive models for the *C. P*, *E. P* and *P. P*, respectively. Figure 15 shows the PRS results of the three predictive models,

$$\begin{aligned} C.P\,(P,T,V) = {} & -861.668 - 2037.840P - 7.497T + 58.032V \\ & + 2274.164P^2 - 6.624PT + 12.827PV \\ & + 0.395T^2 - 0.064TV - 0.818V^2 - 554.948P^3 \\ & - 0.403P^2T - 12.840P^2V + 0.109PT^2 \\ & + 0.386PV^2 - 0.002T^3 - 0.003T^2V + 0.001TV^2 \\ & + 0.003V^3 - 0.090PTV, \end{aligned} \tag{9}$$

$$\begin{aligned} E.P\,(P,T,V) = {} & -389.593 - 189.380P + 2.068T + 22.419V \\ & + 96.887P^2 + 22.002PT - 7.837PV - 0.307T^2 \\ & - 0.007TV - 0.338V^2 - 373.147P^3 - 2.159P^2\mathrm{T} \\ & + 10.711P^2\mathrm{V} - 0.093PT^2 - 0.584PV^2 + 0.002T^3 \\ & + 0.002T^2V - 0.0003TV^2 + 0.002V^3 - 0.083PTV, \end{aligned} \tag{10}$$

$$\begin{aligned} P.P\,(P,T,V) = {} & -725.264 - 1710.830P - 21.348T + 48.330V \\ & + 1977.216P^2 - 12.094PT + 12.679PV \\ & + 0.866T^2 - 0.073TV - 0.579V^2 - 88.039P^3 \\ & - 7.987P^2T - 18.167P^2V + 0.151PT^2 \\ & + 0.952PV^2 - 0.004T^3 - 0.007T^2V + 0.003TV^2 \\ & + 0.001V^3 + 0.022PTV. \end{aligned} \tag{11}$$

Figure 16 is the comparison results of the numerical and fitted values of the DOE sample points. It can be seen that the simulation and fitted values of every sample point agree very well. To delve into error and reliability of the prediction models, five sample points are selected in the DOE, randomly changed the influencing parameters to obtain the additional calculation results of five pressure values, and analyzed the error through the data of these 10-point results. The error analyses are shown in Table IV. The table presents that the *MER* of *C. P*, *E.P*, *P.P* are 0.362%, 0.239%, 0.506%, and the *ME* of *C.P*, *E.P*, *P.P* are 0.919%, 0.487%, 2.59%, and the *MER* and *ME* of the predictive model are very small. Meanwhile, the R^2 of the predictive model of the *C. P* (*P*, *T*, *V*), *E. P* (*P*, *T*, *V*), and *P. P* (*P*, *T*, *V*) are 0.9998, 0.9999, and 0.9994, respectively, which are very close to 1. Therefore, according to the *MER*, *ME*, and R^2 values, the predictive models are precise, and they can be applied in the future for related work.

5. The influence of the parameter of temperature (T) on the pressure results

According to the predictive model, the influence of the factors on the pressure values can be obtained conveniently and quickly. Therefore, the impact of the parameter of *T* on the strengths of compression wave and expansion wave and the corresponding peak-peak value will be further examined. Figure 17 shows the pressure wave values changing with *T* under 1 atm and different velocities. It can be seen that with the increase in *T*, both the strengths of compression and expansion values gradually decreases in a nearly linear fashion. Table V shows the reduction rate of the pressure wave values with the *T* increment of 5 °C. For the compression wave, variation of the reduction rate of the compression wave value is approximately 1.1–1.5% (∼1.1%, $30 \le T \le 45$). For the expansion wave, the change range of the reduction rate is approximately 0.4–0.6% (∼0.4%, $30 \le T \le 45$). For the peak-peak value, the change range of the reduction is approximately 0.6–0.8%. The above results indicate that the reduction rate of pressure with *T* is basically determined; therefore, for the different conditions, the pressure values can be predicted.

V. SENSITIVITY ANALYSIS

A. Sensitivity analysis method selection

The basic principle and application range of the sensitivity analysis include a local and global sensitivity analysis. The local sensitivity analysis is only applied to the research factors for the local influence of the model. This analysis method is developed on the linear model; when the model is nonlinear or the ranges of the input factors are on different number levels, the local sensitivity analysis method cannot provide accurate analysis results. Therefore, the local sensitivity analysis method is mainly applied to a simple mathematical model, easily obtaining the sensitivity coefficient and fewer uncertain factors. The global sensitivity analysis comprehensively studies the global impact of various factors on

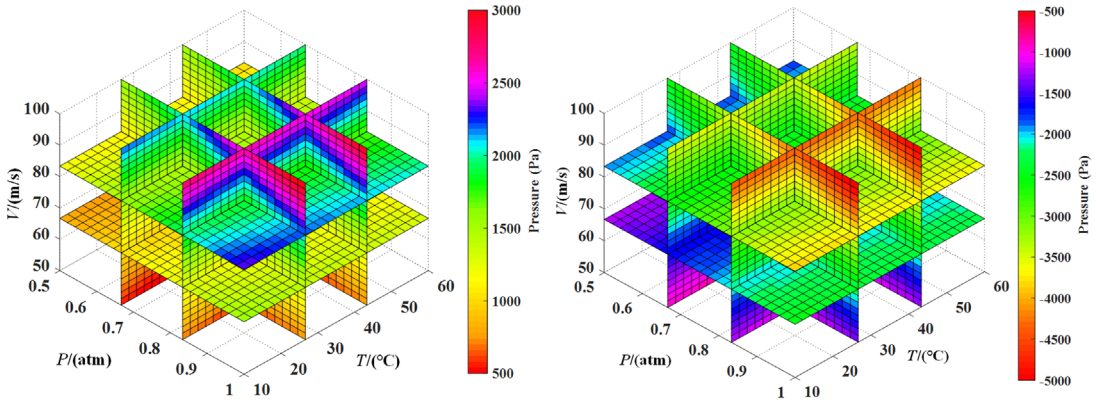

(a) Predictive model of *C. P*

(b) Predictive model of *E. P*

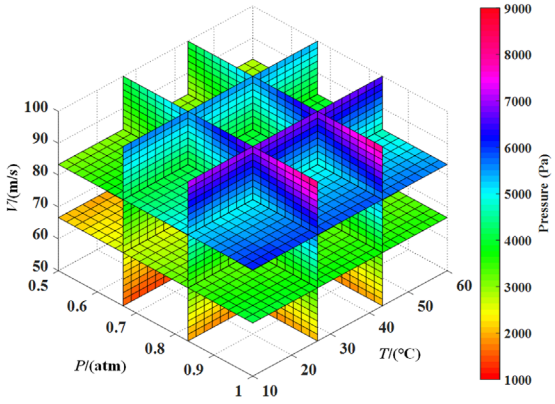

(c) Predictive model of *P. P*

FIG. 15. The PRS predictive model results of three pressure values.

the model. It can provide more comprehensive analysis on the parameter sensitivity and is not limited by the model. Therefore, the global sensitivity analysis method has stronger applicability and generality and has received more extensive attention in the industry.[28]

Common global sensitivity analysis methods include the Morris method, FAST method, GLUE method, Sobol method and extended FAST method, where the Sobol method is based on the principle of variance decomposition and can be used for nonlinear and nonmonotonic mathematical models. The Sobol method has strong computing power and convenience, can calculate the sensitivity coefficient of input parameters of any dimension and the influence of the coupling effect between parameters, and has strong applicability to nonlinear models. Therefore, in this study, the Sobol method is selected as the sensitivity analysis method.

B. Sobol sensitivity analysis method

1. Application to the predictive model

To make the corresponding theory clearer, the following description is in particular, made. Sobol sensitivity captures the effects of interactions between nonlinear responses and test parameters through a global approach, which has the advantage of testing the sensitivity of the entire space. The Sobol method can express the form of the functional model $Y = f(x)$, where Y is the output of the scalar, $f(x)$ is a square integrable function, $x = (x_1, x_2, \ldots, x_n)$ is n dimensional parameters and x is uniformly distributed in [0, 1]. This research focuses on three parameters, and therefore $n = 3$. The pressure value predictive model of this research can be shown as

$$Y = f(h), \tag{12}$$

where $h = (h_1, h_2, \ldots, h_n)$. An n-dimensional element body R^{n} must be defined as the spatial domain of the input parameters. R^{n} can be expressed as

$$R^n = (h_i | 0 \le h_i \le 1;\ i = 1, 2, \ldots, n). \tag{13}$$

According to the Sobol decomposition method, the equation $Y = f(h)$ can be decomposed into situations of increasing order,

$$Y = Y_0 + \sum_{i=1}^{n} Y_i + \sum_{i=1}^{n} \sum_{j>1}^{n} Y_{ij} + \cdots + Y_{1,2,\ldots,n}, \tag{14}$$

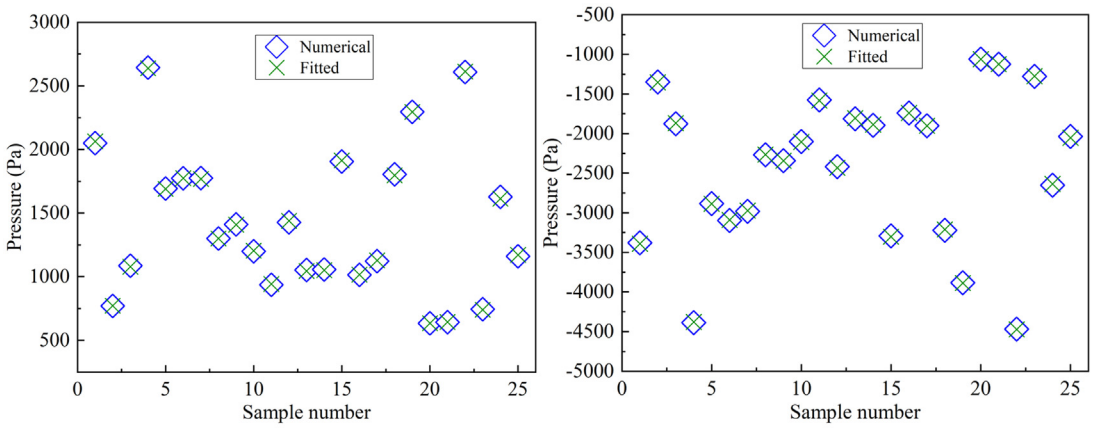

(a) The comparison of *C. P* (b) The comparison of *E. P*

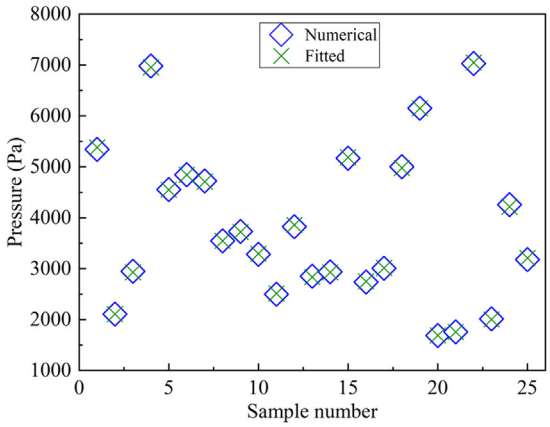

(c) The comparison of *P. P*

FIG. 16. Comparison of numerical and fitted values of DOE sample points.

TABLE IV. Error analysis of the predictive model.

Models	*MER* (%)	*ME* (%)	*RMSE*	R^2
C.P (*P*, *T*, *V*)	0.362	0.919	6.832	0.9998
E.P (*P*, *T*, *V*)	0.239	0.487	6.630	0.9999
P.P (*P*, *T*, *V*)	0.506	2.589	34.658	0.9994

where Y_0 is the expected value of the total model based on the corresponding input parameters. $Y_i = Y(h_i)$ is the function value corresponding to the ith error term h_i. $Y_{ij} = Y(h_i, h_j)$ represents the function value corresponding to the combined action of the error terms h_i and h_j.

Calculate the variance of Eq. (14) and divide both ends by the total variance for orthogonal transformation to obtain

$$\sum_{i=1}^{n} S_i + \sum_{i=1}^{n}\sum_{j>i}^{n} S_{ij} + \cdots + S_{1,2,\ldots,n} = 1. \tag{15}$$

In the equation, S_i is the first-order sensitivity coefficient of the parameter h_i, and the first-order sensitivity coefficient is used to measure the influence weight of the input quantity on the overall output. The second-order sensitivity S_{ij} represents the corresponding sensitivity coefficient for the coupling effect of parameters h_i and h_j.

To evaluate whether the coupling influence between the input terms can be ignored, it is usually necessary to introduce the overall sensitivity coefficient S_{Ti} to further evaluate the overall influence of the error term h_i. The overall sensitivity coefficient S_{Ti} can be simply regarded as the sum of the first-order sensitivity coefficient S_i of h_i and all the higher-order sensitivity coefficients coupled with h_i.

2. Monte Carlo estimate

The input parameters need to be quasi-Monte Carlo sampled by the Sobol method before the sensitivity analysis to generate two mutually independent $k \times n$ sampling matrices A and B, where k is the sampling quantity of every input parameter and n is the input parameter quantity. At the same time, matrices $A_B^{(i)}$ and $A_B^{(i)}$ must be defined,

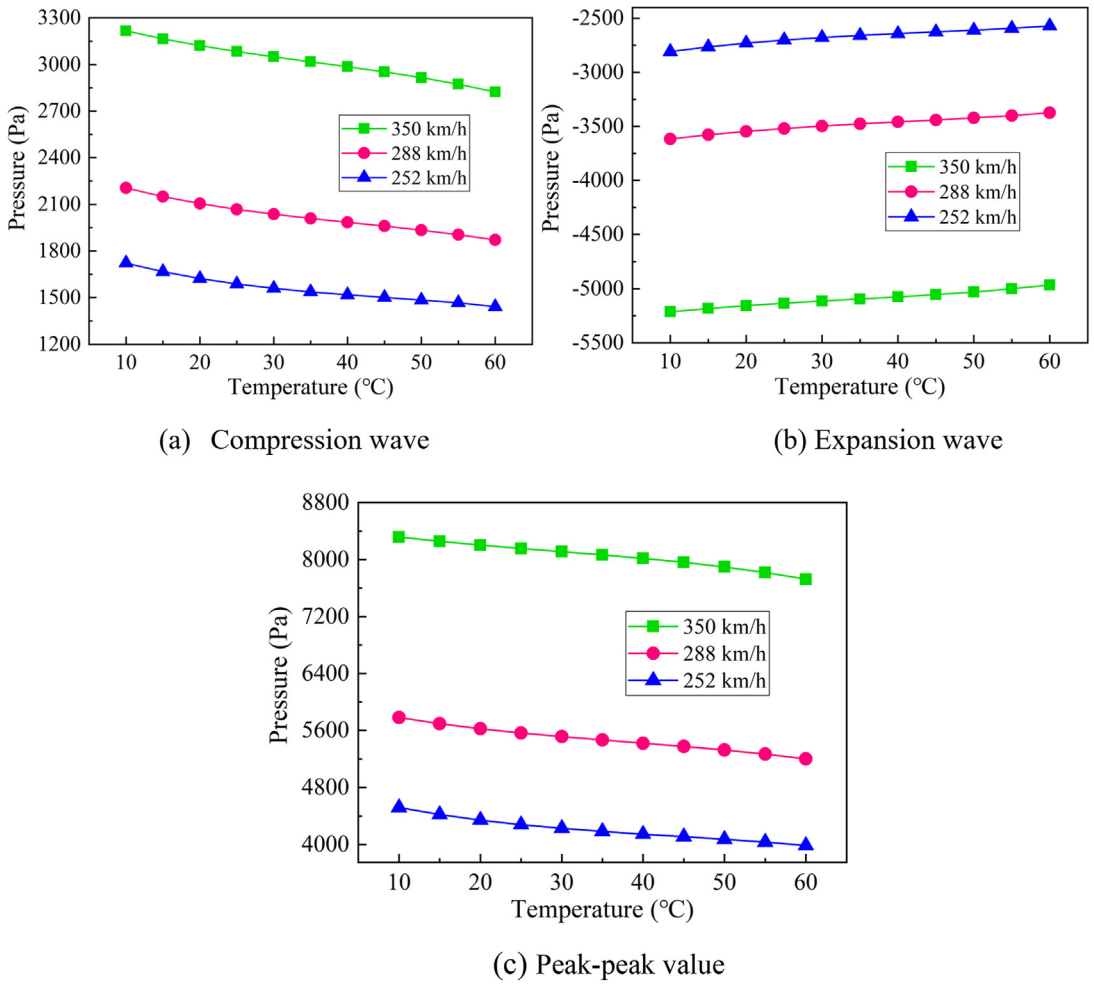

FIG. 17. The change of pressure values with parameter of temperature.

TABLE V. The reduction rate of the pressure values with parameter of temperature.

	C.P		E.P		P.P	
Temperature (°C)	Value (Pa)	Reduction rate (%)	Value (Pa)	Reduction rate (%)	Value (Pa)	Reduction rate (%)
10	3214.1	...	−5214.3	...	8318.4	...
15	3165.1	1.548	−5183.2	0.600	8256.5	0.750
20	3121.6	1.394	−5157.1	0.506	8203.5	0.646
25	3083.7	1.229	−5134.9	0.432	8156.2	0.580
30	3049.9	1.108	−5114.9	0.391	8111.6	0.550
35	3017.8	1.064	−5096	0.371	8066.6	0.558
40	2986.0	1.065	−5076.5	0.384	8017.9	0.607
45	2952.5	1.135	−5055.3	0.419	7962.6	0.695
50	2915.5	1.267	−5030.8	0.487	7907.4	0.698
55	2873.1	1.476	−5001.6	0.584	7859.3	0.612
60	2830.5	1.505	−4969.4	0.648	7795.1	0.824

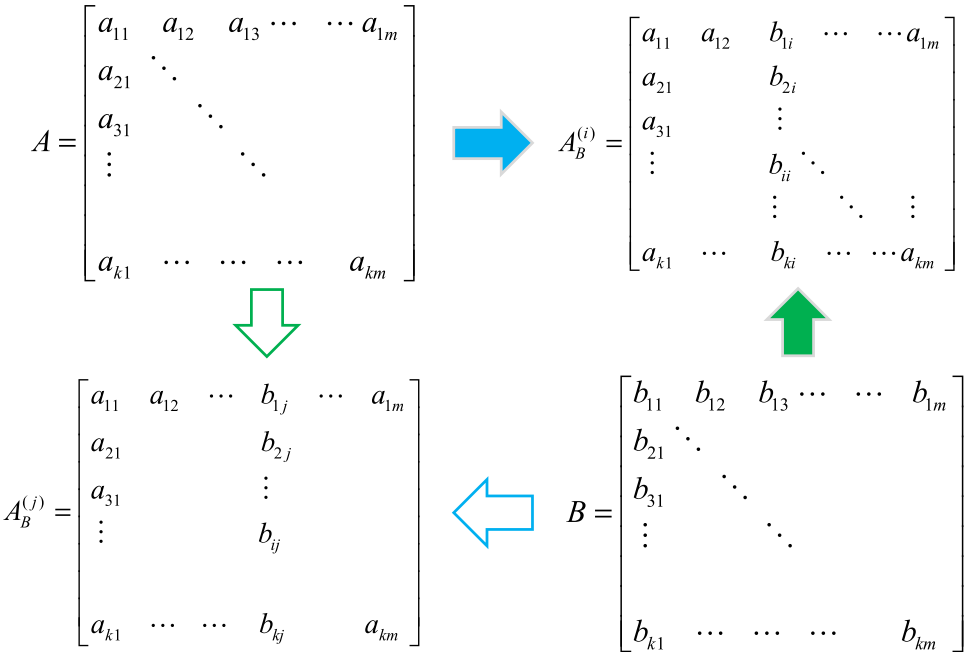

FIG. 18. The process of generating matrices $A_B^{(i)}$ and $A_B^{(j)}$.

which are additionally based on the sampling matrices A and B. The generation process of the matrices $A_B^{(i)}$ and $A_B^{(j)}$ is shown in Fig. 18.

In this research, 2000 sampling points of influence factors can be generated by using the Sobol analysis method, which can obtain two independent 2000×3 sampling matrices A and B. The corresponding matrices $A_B^{(i)}$ and $A_B^{(j)}$ can be further generated by specific matrix transformations for simulation analysis.

C. Sensitivity calculation and analysis

According to Eq. (13), the value range of the influencing parameter is [0, 1]. Therefore, the three parameters P, T, and V should be normalized and placed in the [0, 1] range. After the normalization is completed, the PRS fitting is performed on the sample points again, and a new fitting formula is obtained. An error analysis is carried out using the newly obtained fitting formula, and the obtained results are basically the same as the previous ones, with high accuracy. Then, sensitivity analysis was carried out by the relevant normalized parameters according to the formula.

Figure 19 and Table VI show the results of the sensitivity index to the influencing parameters. Taking the compression wave as an example, the first-order sensitivity indices S_i of the three influencing parameters to the pressure value are 0.2682, 0.0312, and 0.6935, and the compression wave and peak-to-peak sensitivity results are basically the same, so the largest contribution rate of the three parameters to the result is V, the second is P, and the smallest is T. According to Eq. (15), the sum of all sensitivities of all parameters is 1. In this study, the sums of the first-order sensitivities S_i of the three parameters of P, T, and V are 0.9932, 0.9742 and 0.9778, respectively, which are very close to 1. This shows that the higher-order sensitivities of the three parameters are very small and can be ignored.

Figure 19 and Table VI depict that the global index S_{Ti} of each influencing parameter on *C. P*, *E. P* and peak-to-peak is slightly larger than the corresponding first-order index S_i value. The difference between S_i and S_{Ti} of each parameter is relatively small, indicating that the coupling effects among parameters P, T, and V are relatively small, and the interaction between parameters can be ignored, which is the same as the previous conclusion.

In Table VI, the first-order indices of parameter T to the compression pressure, expansion pressure and peak-to-peak are 0.0312, 0.0163, and 0.0181, respectively, indicating that temperature has the greater effect on the initial compressional wave than the peak value of the initial expansion wave. The first-order indices of parameter P to the compression pressure, expansion pressure and peak-to-peak are 0.2692, 0.2765, and 0.2760, respectively, and therefore the atmospheric pressure has basically the same effect on the peak value of the initial expansion wave. The effect on the initial compressional wave is slightly small. At the same time, the first-order indices of parameter V to the compression pressure, expansion pressure and peak-to-peak are 0.6938, 0.6914, and 0.6937, respectively; therefore, the train speed has the same influence on the compression pressure, expansion pressure and peak-to-peak.

Through the above analysis, the weight of the influence of each factor on the pressure result is obtained. In tunnels with large changes in atmospheric pressure and high geothermal, the speed of the train can be properly adjusted according to the local temperature and atmospheric pressure so that the pressure of the train can be relieved to a certain extent. The scientific realization of passenger comfort under the condition of reasonable adjustment of train speed. These research results can provide important technical support for the mitigation technology of pressure waves.

VI. CONCLUSIONS

In this research, predictions of the peak pressure values and analyses of the sensitivity of influencing parameters were carried out in long tunnels with high geothermal properties. First, the initial

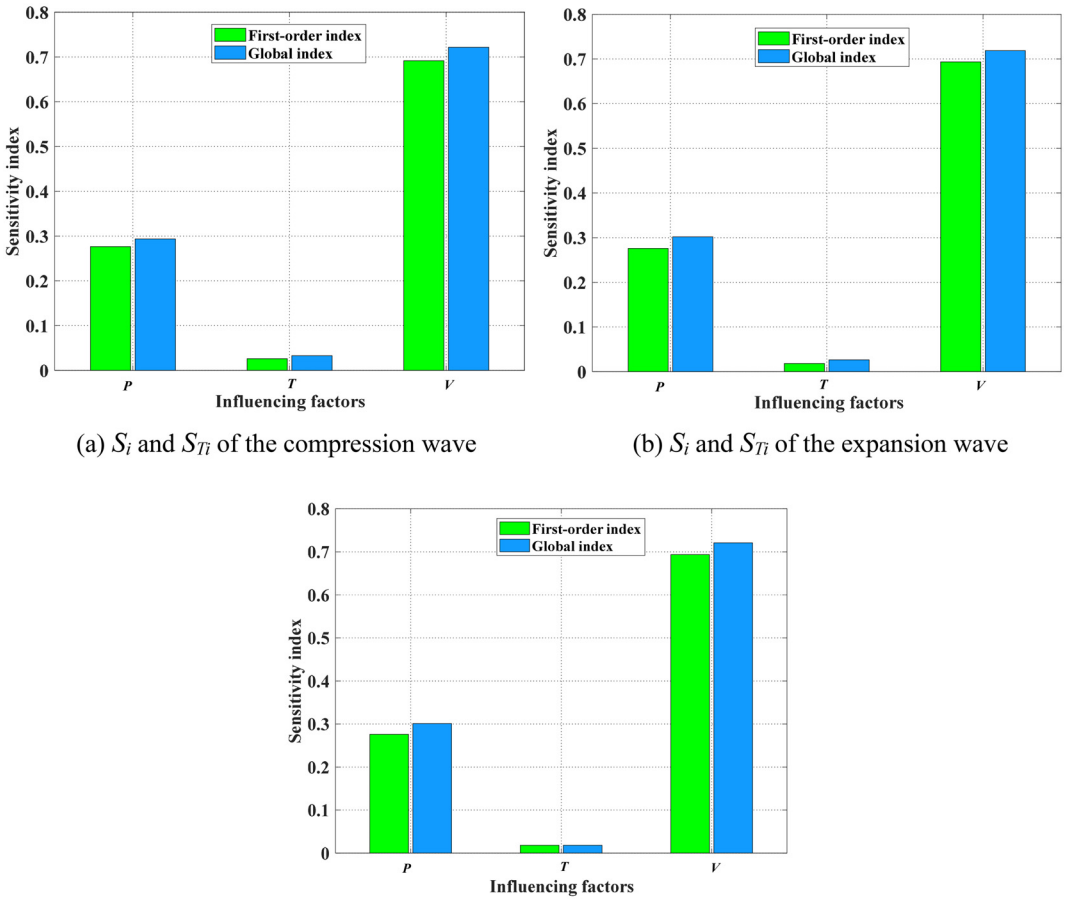

(a) S_i and S_{Ti} of the compression wave

(b) S_i and S_{Ti} of the expansion wave

(c) S_i and S_{Ti} of peak-to-peak

FIG. 19. The S_i and the S_{Ti} of the influencing parameters.

TABLE VI. The value of the sensitivity index.

Sensitivity index	Compression pressure			Expansion pressure			Peak-to-peak		
Parameter	*P*	*T*	*V*	*P*	*T*	*V*	*P*	*T*	*V*
First-order index S_i	0.2682	0.0312	0.6938	0.2765	0.0163	0.6914	0.2760	0.0181	0.6937
Global index S_{Ti}	0.2935	0.0329	0.7215	0.3017	0.0166	0.7186	0.3010	0.0183	0.7208

compression wave value and the initial expansion wave peak value, and the corresponding peak-to-peak value of the pressure wave were predicted by experimental design and the PRS method, and the predictive model was obtained. Then, based on the prediction model, the sensitivity of the influencing parameters was analyzed using the Sobol sensitivity analysis method, and the first-order and global sensitivity coefficients of *P*, *T*, and *V* to the pressure values were obtained. The targeted and reasonable adjustment of parameters can effectively relieve the pressure wave inside the train and improve passenger comfort in geothermal tunnels. The results are detailed as follows:

(1) The PRS method was used to predict the values of the pressure waves, the accuracy of the predictive models was verified, and the coefficient of determination was very close to 1, indicating that the predictive model was reliable.
(2) The result of the sensitivity analysis shows that *V* has the greatest first-order and global sensitivity to pressure results, while *T* has the least effect.
(3) The tunnel temperature *T* has the greater effect on the initial compressional wave value than the initial expansion wave peak value.

(4) The difference between the S_i and the S_{Ti} of each parameter is relatively small, indicating that the coupling effect between parameters P, T, and V is relatively small, and the interaction between parameters can be ignored.

ACKNOWLEDGMENTS

The authors acknowledge the National Natural Science Foundation of China (Grant Nos. 51905547 and 52078199), the National Key R&D Program of China (Grant No. 2020YFA0710903-C), and the Self-Exploration and Innovation Project for graduate students (Nos. 2022ZZTS0158 and CX20220244).

AUTHOR DECLARATIONS

Conflict of Interest

The authors have no conflicts to disclose.

Author Contributions

Junyan Wang: Conceptualization (equal); Data curation (equal); Methodology (equal); Software (equal); Writing – original draft (equal); Writing – review & editing (equal). **Tiantian Wang:** Project administration (equal); Supervision (equal). **Yiping Wang:** Writing – review & editing (equal). **Chihyung Wen:** Writing – review & editing (equal). **Lei Zhang:** Methodology (equal); Software (supporting). **Zhikun Sun:** Software (supporting).

DATA AVAILABILITY

The data that support the findings of this study are available from the corresponding author upon reasonable request.

REFERENCES

[1]Y. P. Hu, M. N. Wang, Q. L. Wang, D. G. Liu, and J. J. Tong, "Field test of thermal environment and thermal adaptation of workers in high geothermal tunnel," Build. Environ. **160**, 106174 (2019).
[2]Q. S. Yang, J. H. Song, and G. W. Yang, "A moving model rig with a scale ratio of 1/8 for high speed train aerodynamics," J. Wind Eng. Ind. Aerodyn. **152**, 50–58 (2016).
[3]L. Zhang, M. Z. Yang, J. Q. Niu, X. F. Liang, and J. Zhang, "Moving model tests on transient pressure and micro-pressure wave distribution induced by train passing through tunnel," J. Wind Eng. Ind. Aerodyn. **191**, 1–21 (2019).
[4]T. T. Wang, F. Wu, M. Z. Yang, P. Ji, and B. S. Qian, "Reduction of pressure transients of high-speed train passing through a tunnel by cross-section increase," J. Wind Eng. Ind. Aerodyn. **183**, 235–242 (2018).
[5]A. Khayrullina, B. Blocken, W. Janssen, and J. Straathof, "CFD simulation of train aerodynamics: Train-induced wind conditions at an underground railroad passenger platform," J. Wind Eng. Ind. Aerodyn. **139**, 100–110 (2015).
[6]J. R. Bell, D. Burton, M. C. Thompson, A. H. Herbst, and J. Sheridan, "Moving model analysis of the slipstream and wake of a high-speed train," J. Wind Eng. Ind. Aerodyn. **136**, 127–137 (2015).
[7]R. S. Iyer, D. H. Kim, and H. D. Kim, "Propagation characteristics of compression wave in a high-speed railway tunnel," Phys. Fluids **33**(8), 086104 (2021).
[8]G. Z. Li, X. Ye, E. Deng, W. C. Yang, Y. Q. Ni, H. He, and W. K. Ao, "Aerodynamic mechanism of a combined buffer hood for mitigating micro-pressure waves at the 400 km/h high-speed railway tunnel portal," Phys. Fluids **35**(12), 126106 (2023).
[9]Y. K. Liu, W. C. Yang, E. Deng, Z. W. Chen, and Y. Q. Ni, "Pressure amplification effect of initial compression waves in circumferential cracks of high-speed railway tunnel linings," Phys. Fluids **35**(6), 066199 (2023).
[10]Y. Y. Ko, C. H. Chen, I. T. Hoe, and S. T. Wang, "Field measurements of aerodynamic pressures in tunnels induced by high speed trains," J. Wind Eng. Ind. Aerodyn. **100**(1), 19–29 (2012).
[11]K. W. Wang, X. H. Xiong, C. Y. Wen, G. Chen, X. F. Liang, H. K. Huang, and J. B. Wang, "Formation and propagation characteristics of a weak shock wave in maglev tube," Phys. Fluids **36**(3), 036120 (2024).
[12]T. Miyachi, M. Iida, and T. Fukuda, "Nondimensional maximum pressure gradient of tunnel compression waves generated by offset running axisymmetric trains," J. Wind Eng. Ind. Aerodyn. **157**, 23–35 (2016).
[13]J. J. Luo, "Aerodynamic effect induced by high-speed train entering into tunnel in high altitude area," J. Southwest Jiaotong Univ. **51**(04), 607–614 (2016).
[14]L. F. Wang, X. H. Zhou, L. L. Tao, Y. H. Zeng, and X. C. Ren, "Anti-freezing system of high altitude and high geothermal tunnel based on air-source heat extraction and case analysis," Case Stud. Therm. Eng. **32**, 101832 (2022).
[15]Z. Y. Dai, T. Li, W. H. Zhang, and J. Y. Zhang, "Research on the aerodynamic characteristics of high-speed trains in different altitude environments," J. Mech. Eng. (published online).
[16]X. H. Zhou, X. C. Ren, X. Q. Ye, L. L. Tao, Y. H. Zeng, and X. R. Liu, "Temperature field and anti-freezing system for cold-region tunnels through rock with high geotemperatures," Tunneling Underground Space Technol. **111**, 103843 (2021).
[17]Y. Zeng, K. Liu, X. Zhou, and L. Fan, "Tunnel temperature fields analysis under the couple effect of convection-conduction in cold regions," Appl. Energy **120**, 378–392 (2017).
[18]X. H. Zhou, Y. H. Zeng, and L. Fan, "Temperature field analysis of a cold-region railway tunnel considering mechanical and train-induced ventilation effects," Appl. Energy **100**, 114–124 (2016).
[19]P. Ricco, A. Baron, and P. Molteni, "Nature of pressure waves induced by a high-speed train travelling through a tunnel," J. Wind Eng. Ind. Aerodyn. **95**(8), 781–808 (2007).
[20]M. Liu, C. Zhu, H. Zhang, W. Zheng, S. You, P. E. Campana, and J. Yan, "The environment and energy consumption of a subway tunnel by the influence of piston wind," Appl. Energy **246**, 11–23 (2019).
[21]J. Y. Wang, T. T. Wang, M. Z. Yang, B. S. Qian, L. Zhang, X. D. Tian, and F. C. Shi, "Research on the influence of different heating zone lengths on pressure waves and a newly designed method of pressure wave mitigation in railway tunnels," Tunneling Underground Space Technol. **122**, 104379 (2022).
[22]J. Q. Niu, D. Zhou, X. F. Liang, T. H. Liu, and S. Liu, "Numerical study on the aerodynamic pressure of a metro train running between two adjacent platforms," Tunneling Underground Space Technol. **65**, 187–199 (2017).
[23]Y. B. Lu, X. M. Wu, T. T. Wang, Y. F. Gong, J. C. Zhou, D. W. Chen, H. K. Li, L. Zhang, F. C. Shi, and J. B. Wang, "Study on the adaptive relationship between train nose lengths and variable-section tunnel parameters: Aiming at mitigating micro-pressure waves," Phys. Fluids **36**(5), 056112 (2024).
[24]W. H. Li, T. H. Liu, X. S. Huo, Z. W. Chen, Z. J. Guo, and L. Li, "Influence of the enlarged portal length on pressure waves in railway tunnels with cross-section expansion," J. Wind Eng. Ind. Aerodyn. **190**, 10–22 (2019).
[25]J. Y. Wang, T. T. Wang, M. Z. Yang, B. S. Qian, and K. W. Wang, "Effect of localized high temperature on the aerodynamic performance of a high-speed train passing through a tunnel," J. Wind Eng. Ind. Aerodyn. **208**, 104444 (2021).
[26]Y. Zhang and X. F. Li, "Response-surface-model based on influencing factor analysis of subway tunnel temperature," Build. Environ. **160**, 106140 (2019).
[27]S. C. Xie, H. H. Li, C. X. Yang, and S. G. Yao, "Crashworthiness optimisation of a composite energy-absorbing structure for subway vehicles based on hybrid particle swarm optimization," Struct. Multidisc. Optim. **58**, 2291–2308 (2018).
[28]X. C. Zou, "Sensitivity analysis of geometric error and research of on-machine error compensation for three-axis ultra precision turning machine tool," Ph.D. dissertation (Harbin Institute of Technology, Harbin, 2018).